Colloids and Surfaces A 604 (2020) 125325

Contents lists available at ScienceDirect

Colloids and Surfaces A

journal homepage: www.elsevier.com/locate/colsurfa

New pyrazole derivatives as effective corrosion inhibitors on steel-electrolyte interface in 1 M HCl: Electrochemical, surface morphological (SEM) and computational analysis

Siham El Arrouji[a], Khalid Karrouchi[b,*], Avni Berisha[c,d], Khadija Ismaily Alaoui[a], Ismail Warad[e], Zakia Rais[a], Smaail Radi[f], Mustapha Taleb[a], M'hammed Ansar[g], Abdelkader Zarrouk[h,*]

[a] Laboratory of Engineering, Electrochemistry, Modeling and Environment (LIEME), Faculty of Sciences, University Sidi Mohamed Ben Abdellah, Fez, Morocco
[b] Laboratory of Analytical Chemistry and Bromatology, Faculty of Medicine and Pharmacy, Mohammed V University, Rabat, Morocco
[c] Chemistry Department of Natural Sciences Faculty, University of Prishtina, rr. "NënaTereze" nr.5, 10000, Prishtina, Kosovo
[d] Materials Science - Nanochemistry Research Group, NanoAlb – Unit of Albanian Nanoscience and Nanotechnology, Tirana, Albania
[e] Department of Chemistry and Earth Sciences, Qatar University, PO Box 2713, Doha, Qatar
[f] Laboratory of Applied Chemistry and Environment (LCAE), Department of Chemistry, Faculty of Sciences, University Mohamed Premier, Oujda 60000, Morocco
[g] Laboratory of Medicinal Chemistry, Faculty of Medicine and Pharmacy, Mohamed V University, Rabat, Morocco
[h] Laboratory of Materials, Nanotechnology and Environment, Faculty of Sciences, Mohammed V University, Av. Ibn Battuta. P.O. Box 1014, Rabat, Morocco

GRAPHICAL ABSTRACT

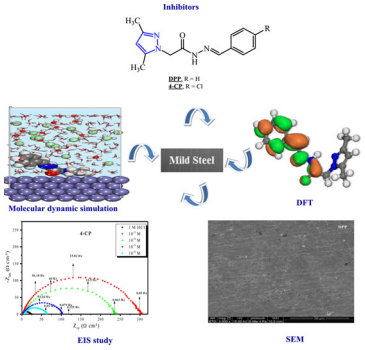

ARTICLE INFO

Keywords:
Pyrazole derivatives
Mild steel corrosion
Electrochemical techniques
SEM
DFT/MD

ABSTRACT

Corrosion inhibition is a vast area of research and its development is attracting increasing attention from researchers. Given the different biological activities that present these compounds, in the present work, we investigated two dimethyl-1*H*-pyrazole derivatives namely: (*E*)-*N*′-benzylidene-2-(3,5-dimethyl-1*H*-pyrazol-1-yl) acetohydrazide (**DPP**) and *E*)-*N*′-(4-chlorobenzylidene)-2-(3,5-dimethyl-1*H*-pyrazol-1-yl)acetohydrazide (**4-CP**) as corrosion inhibitors for mild steel (MS) in 1 M HCl using weight loss (WL), electrochemical techniques [potentiodynamic (PP) polarization, electrochemical impedance spectroscopy (EIS)], surface examinations by scanning electron microscopy (SEM). Theoretical studies such as quantum chemical and molecular simulations studies were used to support the experimental findings. Analyses on mass loss (ML) and electrochemical properties confirmed adsorption of inhibitor as a protective layer on the surface of MS. The inhibition efficiency of **DPP** and **4-CP** was enhanced as the concentration of inhibitors increased but decrease with rising temperature. The maximum inhibition efficiency for **DPP** and **4-CP** at 10^{-3} M concentration has been obtained 80 % and

* Corresponding authors.
E-mail addresses: khalid.karrouchi@um5s.net.ma (K. Karrouchi), azarrouk@gmail.com (A. Zarrouk).

https://doi.org/10.1016/j.colsurfa.2020.125325
Received 4 May 2020; Received in revised form 17 July 2020; Accepted 20 July 2020
Available online 22 July 2020

94 % respectively. Analysis of adsorption isotherms revealed that adsorption of **DPP** and **4-CP** on MS surface follows Langmuir isotherm. Potentiodynamic polarization study confirmed that **DPP** and **4-CP** are of mixed-kind inhibitors. EIS investigations displayed that the polarization resistance raised to 93.7 Ω cm^2 and 287.7 for **DPP** and **4-CP**, respectively at 10^{-3} M. Furthermore, to get detailed electronic/atomic-level findings regarding the dimethyl-1*H*-pyrazole derivatives interactions over the MS substrate, theoretical investigations applying molecular dynamics (MD) and density functional theory (DFT) methods were conducted. The results extracted from these approaches affirmed the **DPP** and **4-CP** adsorption on the MS adsorbent.

1. Introduction

Corrosion of metals in acidic environments has been the concern of engineers in industrial regions [1]. Carbon steel alloys because of their versatile character and reasonable price have been widely considered, particularly in oil and gas pipelines with high risks because of being subjected to corrosive media [2]. Corrosion is a chemical, electrochemical or sometimes biological reaction taking place between the metal and the surrounding environment. There are multifarious reasons/mechanisms behind corrosion phenomenon to be precisely detected and controlled for the sake of protection of metals against corrosive moieties [3]. The corrosion inhibition of carbon steel surfaces in acidic solutions, especially hydrochloric acid (HCl) playing an important role in economics. HCl solutions are used extensively in chemical and several industrial processes such as acid cleaning, pickling, descaling and oil wet cleaning. Nowadays, the use of corrosion inhibitors is one of the most effective and well-known routes to keep corrosion in aqueous solutions under control [4]. Following the need for corrosion detection and protection, various organic and inorganic corrosion inhibitors have been examined in proper concentration in corrosive environment to reduce the rate of inevitably taking place electrochemical corrosion [5]. Nevertheless, designing proper corrosion inhibitors necessitates both the knowledge and experience. Typically, corrosion prevention systems are grounded on the development of inhibitors with minimum environmental risk and toxicity [5,6]. In addition, synthetic inhibitors mostly have active functional groups e.g. hydroxyl, amine and π -electron, that make possible physical or chemical adsorption on the surface of metals [7]. Due to the adsorption of inhibitors on the surface of the substrate, a physical barrier layer forms that protect metals from the corrosion [8]. These species are added with a small amount to decrease the reactivity of environments. The efficiency and the adsorption capacity of the inhibitors are related to their molecular structures, their spatial planarity's, the natures of the functional groups and their attractions. Various chemical compounds of organic or inorganic synthesis are used as structures with polar functions of heteroatoms (S, O, N, etc…), heterocyclic electrons and/or π [9–17], and are considered as responsible for the process adsorption of the compounds.

The choice of the compounds studied is therefore based, on their possible inhibitory power on the one hand, which can be linked to their structure containing several active absorption centers, such as heteroatoms (N, O) and aromatic nuclei, in the other hand, pyrazole-based heterocycles have a wide range of biological activities as an anti-inflammatory, antidepressant, against rheumatoid arthritis, antibacterial, anticonvulsant and their use as herbicides, fungicides, pesticides, insecticides and dyes [18–27].

Given these very important biological properties of these compounds, in the present work and with the aim of continuing of looking for effective inhibitors against corrosion of metals in aggressive environments, namely MS, this new study falls within this framework. In a quest to continue to develop the heterocyclic organic compounds that contain nitrogen and oxygen as corrosion inhibitors for industrial application, (*E*)-*N*′-benzylidene-2-(3,5-dimethyl-1*H*-pyrazol-1-yl)acetohydrazide (**DPP**) and *E*)-*N*′-(4-chlorobenzylidene)-2-(3,5-dimethyl-1*H*-pyrazol-1-yl)acetohydrazide (**4-CP**) have been synthesized. To assess the corrosion inhibition performance of new pyrazole derivatives molecules (**DPP** and **4-CP**) we used potentiodynamic polarization and electrochemical impedance spectroscopy (EIS) tests in 1 M HCl solution. After the corrosion test the surface of the steel was characterized by scanning electron spectroscopy (SEM). Besides the experimental studies, comprehensive computational analyses based on density functional theory (DFT) and molecular dynamics (MD) simulation were employed to uncover the state on interfacial interaction between the **DPP** and **4-CP** molecules and corrosive moieties. The DFT studies were specifically applied to elucidate detailed understandings regarding the local/global reactivity of **DPP** and **4-CP**.

2. Experimental section

2.1. Materials

The molecular structures of the two compounds (**DPP** and **4-CP**) used to fight corrosion are illustrated in Fig. 1. MS is composed of 0.21 % carbon, 0.09 % phosphorous, 0.05 % sulfur, 0.38 % silicon, 0.01 %

IUPAC name and abbreviation	Chemical structure
(*E*)-*N*′-benzylidene-2-(3,5-dimethyl-1*H*-pyrazol-1-yl)acetohydrazide (DPP)	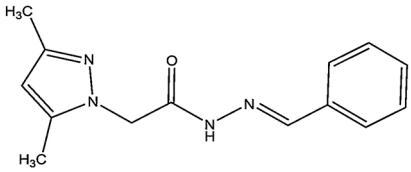
(*E*)-*N*′-(4-chlorobenzylidene)-2-(3,5-dimethyl-1*H*-pyrazol-1-yl)acetohydrazide (4-CP)	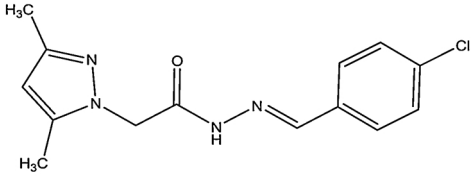

Fig. 1. The chemical structures of inhibitors **DPP** and **4-CP**.

aluminium, 0.05 % manganese, and the remaining is iron. Hydrochloric acid and absolute ethanol obtained from Sigma-Aldrich company were used in preparation of the tested solutions using ultra-pure distilled water. The concentration range of **DPP** and **4-CP** are 10^{-3} M→10^{-6} M.

2.2. Synthesis of inhibitors

The inhibitors **DPP** and **4-CP** were synthesized by reported procedure [28] as shown in Scheme 1. To a solution of acid hydrazide (**1**) (168 mg, 1 mmol) and benzaldehyde (106 mg, 1 mmol) or 4-chlorobenzaldehyde (140.5 mg, 1 mmol) in 10 mL of ethanol was added two drops of acetic acid. The mixture was maintained under reflux for 3 h, until TLC indicated the end of the reaction. Then, the reaction mixture was cooled down to 25 °C, and the precipitate formed was filtered out washed with ethanol and recrystallized from ethanol.

*(E)-N'-benzylidene-2-(3,5-dimethyl-1H-pyrazol-1-yl)acetohydrazide (**DPP**)*

White solid, Yield = 75 %; m.p = 170 − 172 °C; IR (ν(cm^{-1})) : 3369 (NH), 1678 (C = O), 1619 (C = N); ^{1}H NMR: (300 MHz, DMSO-d$_6$, δ(ppm)) : 2.05 (s, 3H, CH_3), 2.13 (s, 3H, CH_3), 5.19 (s, 2H, N − CH_2-), 5.80 (1H, s, H4 pyrazole), 7.41–7.70 (m, 5H, H-phenyl), 8.01 (1H, s, N = CH), 11.59 (s, 1H, NHCO); ^{13}C NMR: (75 MHz, DMSO-d$_6$, δ (ppm)): 11.13 (CH_3), 13.73 (CH_3), 50.82 (-CH_2), 105.21 (C4-pyrazole), 127.60 (C3 & C5-phenyl), 129.28 (C2 & C6-phenyl), 130.45 (C4-phenyl), 134.43 (C1-phenyl), 140.56 (C3-pyrazole), 144.55 (N = CH), 147.94 (C5-pyrazole), 169.04 (C = O). ESI-MS: m/z = 257.2 [M + H]$^+$.

*(E)-N'-(4-chlorobenzylidene)-2-(3,5-dimethyl-1H-pyrazol-1-yl) acetohydrazide (**4-CP**)*

White solid, Yield = 57 %; m.p = 174 − 176 °C; IR (ν(cm^{-1})) : 3397 (NH), 1677 (C = O), 1618 (C = N); ^{1}H NMR: (300 MHz, DMSO-d$_6$, δ(ppm)) : 2.05 (s, 3H, CH_3), 2.12 (s, 3H, CH_3), 5.18 (s, 2H, N-CH_2-), 5.80 (1H, s, H4-pyrazole), 7.48 (d, J = 8.7 Hz, 2H, H3 & H5-Ar), 7.73 (d, J = 8.7 Hz, 2H, H2 & H6-Ar), 8.20 (1H, s, N = CH), 11.67 (s, 1H, NHCO); ^{13}C NMR: (75 MHz, DMSO-d_6, δ (ppm)): 11.05 (CH_3), 13.73 (CH_3), 50.81 (-CH_2), 105.33 (C4 pyrazole), 129.24 (C3 & C5-Ar), 129.35 (C2 & C6-Ar), 133.48 (C1-Ar), 135.09 (C4-Ar), 140.55 (C5 pyrazole), 143.15 (C3 pyrazole), 146.34 (N = CH), 169.13 (C = O). ESI-MS: m/z = 291.0 [M + H]$^+$.

2.3. Method and techniques used for corrosion testing

2.3.1. Mass loss method (ML)

MS coupons (1.5 × 1.5 × 0.08 cm^3) were polished using emery sheets of different grades after that they were degreased in acetone for 10 min in an ultrasonic water bath. Subsequently, the rinsed and dried MS coupons were weighed using four digits analytical balance. The concentration range of **DPP** and **4-CP** are 10^{-3} M→10^{-6} M. However, a blank solution was composed of 1 M HCl solution. The weighed coupons were immersed simultaneously in both blank and test solutions and withdrawn after every 360 min in a 100 mL solution. These coupons were washed and dried in air before reweighing. The surface coverage (θ) and percentage inhibition (η_{ML}%) were determined from weight loss data using Eq.s (1) and (2), respectively.

$$\theta = \frac{w_0 - w_i}{w_0} \quad (1)$$

$$\eta_{ML}(\%) = \theta \times 100 \quad (2)$$

where the weight loss of these coupons with and without the addition are represented **DPP** and **4-CP** by w_i and w_0, respectively [29].

2.3.2. Electrochemical techniques

Tafel polarization and electrochemical impedance parameters were collected with the help of

PGZ 100 as an electrochemical instrument equipped with Volta master 4.0 software. These measurements were preceded in a classical three electrode cell with an overall volume of 100 mL. The used reference and counter electrodes were saturated calomel electrode and graphite electrode, respectively. Potentiodynamic polarization curves were employed by varying the working electrode potential automatically and the logarithmic current density was plotted against the potential of this working electrode. These polarization branches possess Tafel type behavior for the applied cathodic and anodic potentials and all the electrochemical experimental results. The electrode was immersed for 30 min in the tested solution to provide enough time for E_{corr} to reach a stable value. The polarization curves were recorded by shifting the electrode potential automatically from -650 to − 250 mV with a scanning rate of 0.5 mV/s.

The corrosion inhibition percentage ($\eta_{Logi\text{-}E}$%) was determined by using Eq. (3) [30]:

$$\eta_{Logi-E}(\%) = \frac{i^0_{corr} - i^i_{corr}}{i^0_{corr}} \times 100 \quad (3)$$

where I_{corr} i^0_{corr} and I'_{corr} i^i_{corr} are the corrosion currents without or with the addition of **DPP** and **4-CP** to 1 M HCl solution, respectively.

Measurements of EIS were done at the open circuit potential for MS electrode in 1 M HCl solutions with and without the addition of the different concentrations of **DPP** and **4-CP**. The frequency range (100 kHz – 0.01 Hz) with a root mean square (RMS) amplitude of 10 mV was applied. Fitting of the obtained data to the suggested equivalent circuit was done by ZView software version 2.80.

The inhibition percentage is determined from EIS measurements by Eq. (4):

$$\eta_{EIS}(\%) = \frac{R^i_p - R^0_p}{R^i_p} \times 100 \quad (4)$$

where R_{ct} R^0_p and R'_{ct} R^i_p are the polarization-resistance without or with the addition of **DPP** and **4-CP** in 1 M HCl solution, respectively.

2.4. Surface analysis: SEM

The influence of acid corrosion (1 M HCl) and the addition of **DPP** and **4-CP** (10^{-3} M) on morphology of the surface layer of MS coupons were tested by utilizing scanning electron microscope (SEM) supplied from a FEI Company (Model: FEI ESEM Quanta 450 FEG) typically operated with an acceleration voltage of 20 kV. The preparation of MS coupons was done as described in the ML method.

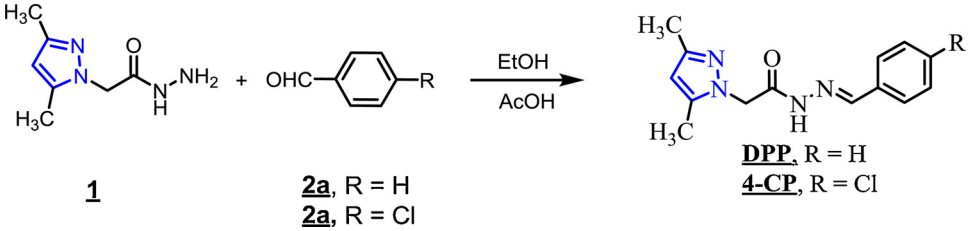

Scheme 1. Scheme 1 for the synthesis of **DPP** and **4-CP.**

2.5. Calculation details

2.5.1. DFT calculations

The calculations DFT were performed using the Dmol3 code. For the geometry optimization the double numerical plus polarization basis set (DNP) is used in combination with the M11-L functional [31] within m-GGA [32,33]. The solvent effect (water) is included by the use of COSMO model [34].

2.5.2. Monte Carlo and molecular dynamic simulation details

For the Monte Carlo (MC) and Molecular dynamic (MD) simulation, the interaction of the iron surface and inhibitor molecules (**DPP** or **4-CP**) in the simulated corrosion media is performed via the Fe(110) model (with periodic boundary condition) with size of: 14.89 Å × 14.89 Å × 6.45 Å with the inclusion of a 25 Å vacuum layer at C axis inclosing 230 water molecules/1 inhibitor molecule (**DPP** or **4-CP**) /15 hydronium + 15 chloride ions. The temperature cycling in MC calculations is varied successively from 10^5 to 10^2 K during the 10 applied cycles (of 1500 steps) after which the lowest possible energy configurations were obtained at decreased temperatures. Before the MD simulations, simulation system optimized via the Smart optimization algorithm until the energy meet the10^{-4} kcal/mol threshold. MD was conducted using an NVT canonical ensemble at 298 K, with a 1 fs time step and a simulation time of 500 ps. The Berendsen thermostat [35] is used for temperature controll. COMPASSII force field [36] as the one of most used forcefield in corrosion studies is used for the simulations [37,38]. The Radial Distribution Function (RDF) analysis, included the whole trajectory.

3. Results and discussion

3.1. Potentiodynamic polarization

The potentiodynamic polarization behavior of Fe-MS in 1 M HCl solution in the presence and absence of **DPP** and **4-CP** is shown in Fig. 2. The related electrochemical parameters such as corrosion potential (E_{corr}), Tafel cathodic and anodic constants (β_c and β_a respectively) and corrosion current density (i_{corr}) were listed in Table 1. The cathodic Tafel curves are in the form of parallel lines, showing that the addition of **DPP** and **4-CP** doesn't adjust the hydrogen evolution mechanism and the decrease of hydrogen ions on the MS surface happens basically across a charge transfer mechanism [39]. The adsorbed inhibitor molecules are first adsorbed onto the surface and acted by merely preventing the reaction sites of the MS surface without affecting the anodic and cathodic reaction mechanism [40]. For anodic Tafel curves, Over the −350 mV, the anodic segments are nearly the equivalent for every one of the concentrations and and they are greater than that of the 1 M HCl segment. This occurrence is in the most part connected with the huge dissolution of the MS, which prompts desorption of the inhibitor molecules from MS surface. This shows that the desorption rate is much more than that of adsorption.

Table 1
Corrosion parameters of potentiodynamic polarization of Fe-MS in the absence and presence of different concentrations of **DPP** and **4-CP** in 1 M HCl.

Medium	Conc. (M)	-E_{corr} (mV_{SCE})	i_{corr} ($\mu A\ cm^{-2}$)	-β_c ($mV\ dec^{-1}$)	β_a ($mV\ dec^{-1}$)	η_{Logi-E} (100)
1 M HCl	––	454 ± 0.5	1947.7 ± 1.7	183	152	–
DPP	10^{-3}	464 ± 0.6	464.4 ± 0.8	190	102	76.2
	10^{-4}	449 ± 0.5	615.9 ± 0.8	201	117	68.4
	10^{-5}	455 ± 0.2	770.2 ± 0.7	182	135	60.6
	10^{-6}	465 ± 0.3	1144.1 ± 1.8	194	120	41.3
4-CP	10^{-3}	436 ± 0.2	134.1 ± 0.5	245	92	93.1
	10^{-4}	453 ± 0.4	215.6 ± 0.4	193	66	88.9
	10^{-5}	457 ± 0.4	458.2 ± 0.8	172	78	76.5
	10^{-6}	458 ± 0.2	642.4 ± 0.7	190	75	67.0

Review of Table 1 uncovers that values of i_{corr} for MS in the presence of **DPP** and **4-CP** are inferiors to that in the uninhibited electrolyte, and the (η_{Logi-E} %) increments strongly with the increasing concentration of **DPP** and **4-CP** molecules. The protection efficiency acquired from polarization measurements is follows the following order: **4-CP** > **DPP**, which can be attributed by the intermolecular transfer of charge increases by the functionalization by a Cl group in the compound **4-CP**.

We can characterize an inhibitor as cathodic or anodic sort if the difference in corrosion potential is in excess of 85 mV relative to that of the 1 M HCl [41]. In our case the, displacement shall not exceed 85 mV. This can be translated that the both salts act as mixed type inhibitors. However, the values of slope (β_c) change with the salts addition pointing to an alteration of the process of cathodic hydrogen developments, which recommend that the studied **DPP** and **4-CP** effectively hinder the corrosion process of MS [42]. The deletion of cathodic procedure can be because of the covering of the surface with monolayer as a result of adsorbed inhibitor molecules. Also, the introduction of **DPP** and **4-CP** modified the value of the anodic Tafel slopes (β_a) with respect to those achieved in blank, which proposes that studied can influence the kinetics of the anodic mechanism. This occurrence is in the most part connected with the huge dissolution of the MS, which prompts desorption of the inhibitor molecules from metal surface. This shows that the desorption rate is much more than that of adsorption [43].

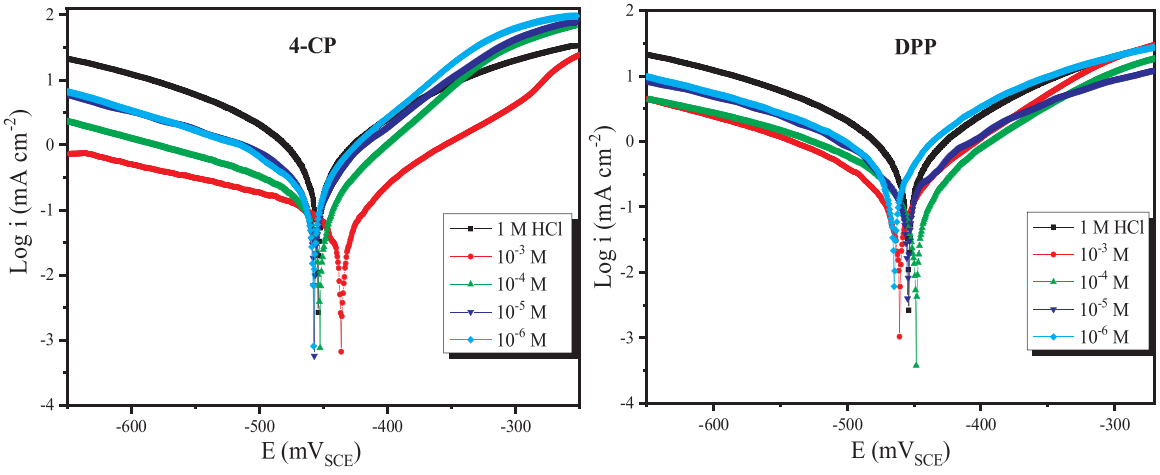

Fig. 2. Tafel curves of MS corrosion with and without of different concentrations of **DPP** and **4-CP** in 1 M HCl.

3.2. Electrochemical impedance spectroscopy studies

EIS technique was used to describe the complex and fundamental mechanisms intervening in the processes involved at the metal/solution interface [44]. This technique is specifically adapted to the determination of the mechanism of action of the inhibitory molecules, thus it allows evaluating the dielectric characteristics of the formed film [45]. Nyquist and Bode diagrams for the corrosion of MS in the 1 M HCl and in the presence of **DPP** and **4-CP** are illustrated in Figs. 3 and 4, respectively. The visual analysis and the observations made in Fig. 3 shows that the Nyquist diagrams appeared with a single capacitive semicircle and the diameter of the latter increases with the concentration of **DPP** and **4-CP**, indicating an increase in the inhibitory capacity of **DPP** and **4-CP** against MS corrosion [46], the diameters of the diagrams of the inhibitor **4-CP** at different concentrations are greater than the inhibitor **DPP** which implies that the **4-CP** is more effective than the **DPP**. This behavior shows that the corrosion process of MS with and without inhibitor species is essentially controlled by the transfer of charge mechanism [47]. In addition, the capacitive loops drawn in Fig. 3 are not perfect semicircles, which may be a result of the frequency dispersion of the interfacial impedance due to the heterogeneity and roughness of the MS surface [48]. The Bode plots are also drawn in Fig. 4, it is clear that the values of the phase angle increase in accordance with the concentration of **DPP** and **4-CP**. These values in the presence of **DPP** and **4-CP** are higher than the blank values, indicating the protective effect of **DPP** and **4-CP** in the oxidation process of MS [49]. Additionally, they are less than 90°, which indicates more clearly the non-ideal behavior of these systems (CPE) [50]. A single maximum of the phase angle shows that only one-time constant is present, consequently only one relaxation process has taken place in the charge transfer process [51]. Indeed, the slope (s) values of the Bode-representations plots (Fig. 4) for intermediate frequency values were not equal to the opposite of unity (-1) [ideal capacitor]. This can attributed to the frequency dispersion of interfacial impedance. The Nyquist and bode representations prove that the addition of **DPP** and **4-CP** to the electrolytic medium did not infect the corrosion process of MS in this medium.

Adjustment of the experimental impedance and bode diagrams for **DPP** and **4-CP** was obtained using the appropriate circuit presented in Fig. 5. This electrical circuit is composed of 3 essential elements: the electrolyte resistance (R_s), the polarization resistance (R_p) and the constant phase element (CPE/n_{dl}) resulting from the non-ideal capacitive behavior of the electronic double layer [52].

The extracted and calculated parameters such as R_s, R_p, double layer capacitance (C_{dl}), and CPE of double layer are listed in Table 2, respectively. The impedance (Z) of the CPE is expressed as follows [53]:

$$Z_{CPE} = Q^{-1}(i\omega)^{-n} \quad (5)$$

where n, ω, Q and i describe the homogeneity degree, the angular frequency (in rad s^{-1}), CPE magnitude and the square root of -1, respectively.

The value of the C_{dl} is calculated using the expression [54]:

$$C_{dl} = [QR_p^{1-n}]^{1/n} \quad (6)$$

From Table 2, it is clear that the values of the R_p increase with the concentration of **DPP** and **4-CP**, while the C_{dl} values decrease for both the **DPP** and **4-CP** inhibitors. With the addition of **DPP** and **4-CP**, the capacity of the double layer (C_{dl}) decreases and goes from 163.3 μF cm^{-2}, for the reference, to 36.8 μF cm^{-2} for a concentration 10^{-3} M of **4-CP** and to 48.9 μF cm^{-2} for the same concentration (10^{-3} M) of **DPP**. This behavior leads to a higher adsorption of the protective molecules on the surface, this adsorption led to the replacement of H_2O molecules by molecules studied at the metal/electrolyte interface [55]. For this effect, the inhibition efficiency obtained makes it possible to block the cathodic and/or anodic active region, this shows that the **DPP** and **4-CP** inhibitors are successful in inhibiting corrosion in a way that more notable [56]. The optimal concentration of 10^{-3} M shows the greatest resistance compared to all the minimum concentrations studied for **DPP** and **4-CP**. And the **4-CP** inhibitor inhibits corrosion better than **DPP**, this result confirms to those obtained by the PDP technique. The diminishing in ***Q*** values by expanding **DPP** and **4-CP** concentration might be credited to the rise in the quantity of adsorbed molecules at steel surface. It is worth pointing that the augment in the deviation parameter (n) values later than the **DPP** and **4-CP** adding, which can be associated to a diminish of surface inhomogeneities caused by adsorption of the **DPP** and **4-CP** molecules on MS surface [57].

3.3. Mass loss measurements method (ML)

3.3.1. Effect of concentration of *DPP* and *4-CP*

Weight reduction is a usually utilized technique to assess the action of inhibitor in corrosion suppressing, and it has high dependability. The corrosion demeanor of MS in 1 M HCl with various doses of **DPP** and **4-CP** was examined by the weight reduction method. The corresponding corrosion rate (*w*) and inhibition efficiency (η_{ML}) are presented in Table 3. As will be seen from Table 3, the *w* value is reduced evidently and η_{ML} is raised after adding **DPP** and **4-CP**. As indicated in Table 3, were found to be that the w of (**4-CP**) is inferior to w (**DPP**). This sort of conduct is commonly linked to the raise in adsorption of the investigated heterocyclic molecules at MS through the blanket of the entire active sites of MS and accordingly a diminution in the speed of degradation of this material [58]. The best η_{ML} values of **4-CP** and **DPP** are 94.1 % and 79.9 %, respectively. In this study MS corrosion is

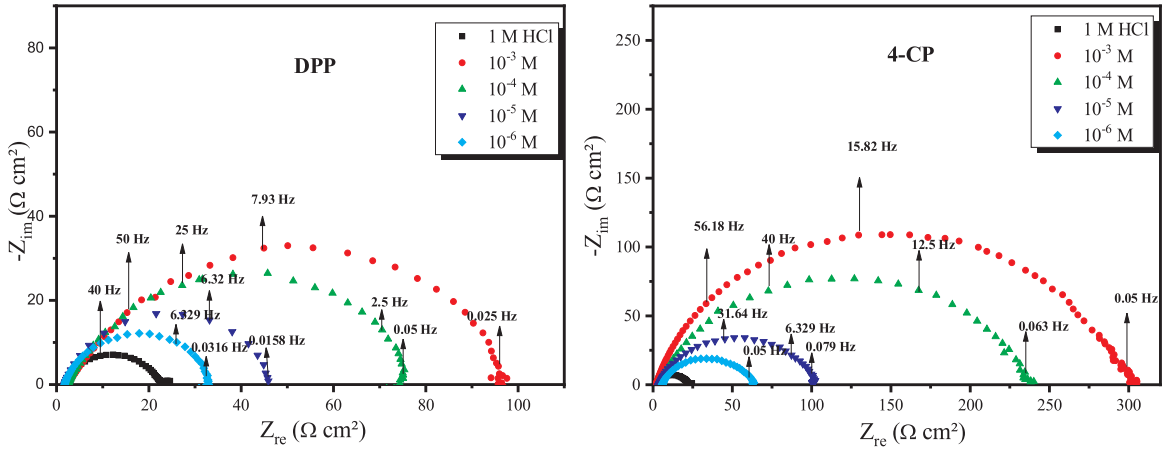

Fig. 3. Nyquist plane impedance diagrams of MS in 1 M HCl without and with **DPP** and **4-CP** at different concentrations.

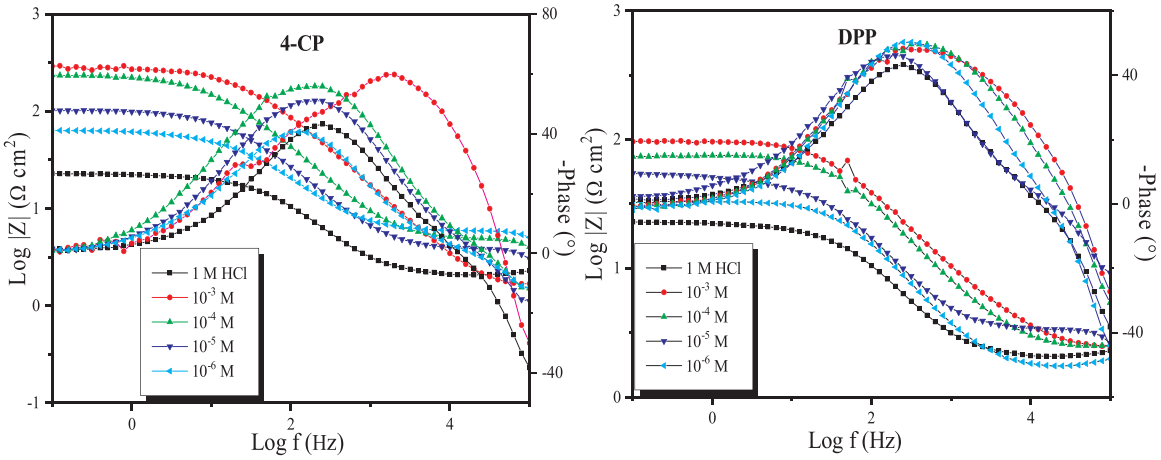

Fig. 4. Bode and phase representations of MS in 1 M HCl without and with **DPP** and **4-CP** at different concentrations.

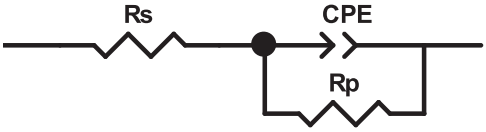

Fig. 5. Adequate equivalent circuit model corresponding to the system studied.

strongly inhibited by **4-CP** (Chloro derivative), which has proven to be the best inhibitor of these two compounds, due to the increase in the delocalization of electronic density in the molecule, which enriches the adsorption sites [59], and gives better inhibition. Aramaki [60] studied the mechanisms of inhibition of benzotriazole and its 5-methyl, 5-chloro and 5-nitro derivatives on copper corrosion, the chloro compound gave the best efficiency, this result was explained by the ease of the formation of the copper complex in the presence of chlorine. So the introduction of chlorine atoms into the molecular structures studied facilitates the adsorption of these molecules on the MS surface. From where: **4-CP** > **DPP**.

3.3.2. *Temperature effect*

In order to confirm the inhibitory protection of **4-CP** and **DPP**, we conducted a study in a temperature range between 308 and 338 K using ML measurements. The ML parameters for MS in molar hydrochloric acid solution only and with 0.001 M of **4-CP** and **DPP** in the temperature interval 308 − 338 K are outlined in Table 4. It can be noted that the recorded *w* value raises in two uninhibited and inhibited electrolytes and the value of inhibiting properties diminish marginally with the expansion in the temperature. This is because of a considerable lessening in adsorption of **4-CP** and **DPP** on the MS surface with ascending temperature and further reason desorption of **4-CP** and **DPP**. Notwithstanding, unmistakably η_{ML} values of **4-CP** decline gradually in comparison to those of **DPP** (at 338 K and in 0.001 M, diminished to 53.0 % for **4-CP** and 33.7 % for **DPP**). These outcomes affirm that **4-CP** displays the best inhibitive properties among these both derivatives in studied temperatures.

Table 3
The corrosion rate and inhibition percentage of the **4-CP** and **DPP** for MS corrosion in 1 M HCl by weight loss method at 298 K.

Medium	Conc. (M)	w (mg cm^{-2} h^{-1})	η_{ML} (%)
1 M HCl	––	0.359 ± 0.005	–
	10^{-3}	0.072 ± 0.005	79.9
	10^{-4}	0.139 ± 0.004	61.3
DPP	10^{-5}	0.225 ± 0.005	37.3
	10^{-6}	0.251 ± 0.003	30.1
	10^{-3}	0.021 ± 0.002	94.1
	10^{-4}	0.036 ± 0.008	90.0
4-CP	10^{-5}	0.072 ± 0.005	79.9
	10^{-6}	0.093 ± 0.007	74.1

The activation parameters that include the activation energy (E_a), the enthalpy of activation (ΔH_a) and the entropy of activation (ΔS_a) were estimated by Arrhenius and transition state relations [61,62] that are given by Eqs (6) and (7), respectively.

$$Rate(w) = Ae^{-E_a/RT} \tag{6}$$

$$Rate(w) = \frac{RT}{Nh} \times e^{\Delta S_a/R} \times e^{-\Delta H_a/RT} \tag{7}$$

where the rate unit is (mg/cm^{-2} h^{-1}), *A* is the frequency factor, *N* is Avogadro's number, *h* is Planck's constant and *R* is the universal gas constant.

Table 2
Electrochemical impedance parameters in the absence and presence of different concentrations of inhibitor molecules at 298 K.

Medium	Conc (M)	R_s (Ω cm^2)	R_p (Ω cm^2)	$10^4 \times Q$ (Ω^{-1} S^n cm^{-2})	CPE		η_{EIS} (%)	θ
					n_{dl}	C_{dl} (μF cm^{-2})		
Blank	1	2.15 ± 0.01	20.0 ± 0.1	4.37 ± 0.04	0.828 ± 0.001	163.3	––	––
DPP	10^{-6}	1.88 ± 0.02	29.8 ± 0.3	3.16 ± 0.03	0.839 ± 0.004	129.1	32.9	0.329
	10^{-5}	1.83 ± 0.02	41.6 ± 0.1	2.28 ± 0.04	0.845 ± 0.006	97.0	51.9	0.519
	10^{-4}	2.61 ± 0.04	71.4 ± 0.5	1.42 ± 0.02	0.850 ± 0.005	63.2	72.0	0.720
	10^{-3}	2.69 ± 0.03	93.7 ± 0.5	1.06 ± 0.01	0.856 ± 0.005	48.9	75.7	0.757
4-CP	10^{-6}	5.69 ± 0.07	57.1 ± 0.4	2.52 ± 0.02	0.842 ± 0.002	113.7	65.0	0.650
	10^{-5}	3.67 ± 0.05	97.3 ± 0.2	1.82 ± 0.04	0.857 ± 0.004	92.8	79.4	0.794
	10^{-4}	4.66 ± 0.05	227.7 ± 1.1	1.05 ± 0.02	0.870 ± 0.007	60.0	91.2	0.912
	10^{-3}	2.02 ± 0.02	287.7 ± 1.0	0.76 ± 0.01	0.887 ± 0.006	36.8	93.0	0.930

Table 4
The WL parameters of MS in 1 M HCl alone, and accomplished an optimum dose of **4-CP** and **DPP** at different temperatures.

Temp. (K)	Medium	w (mg cm^{-2} h^{-1})	η_{ML} (%)
308	1 M HCl	0.736 ± 0.008	––
	DPP	0.240 ± 0.003	67.4
	4-CP	0.086 ± 0.002	88.0
318	1 M HCl	1.471 ± 0.009	––
	DPP	0.641 ± 0.007	56.4
	4-CP	0.265 ± 0.002	82.0
328	1 M HCl	2.634 ± 0.009	––
	DPP	1.554 ± 0.004	41.0
	4-CP	0.759 ± 0.004	71.2
338	1 M HCl	4.039 ± 0.020	––
	DPP	2.678 ± 0.020	33.7
	4-CP	1.898 ± 0.030	53.0

The activation energy of MS in the blank and inhibited solution was achieved from the linear square fits of Ln w vs. (1000/T). While, the values of enthalpy and entropy of activation (ΔH_a and ΔS_a, respectively) were achieved from linear square fits of Ln (w/T) vs. (1000/T) (Fig. 6). The values of E_a, ΔH_a and ΔS_a parameters are given in Table 5.

The obtained value of E_a (49.27 kJ/mol) for MS corrosion in free acidic solution agrees with that mentioned before in previous studies [63]. The activation energy values are increased by the addition of **4-CP** and **DPP** to the acidic blank solution. This confirms their inhibition action by rising the energy barrier of MS corrosion reaction through adsorption of **4-CP** and **DPP** on its surface. This adsorption process renders mass and charge transfer [64]. Data available in Table 5 shows that those positive values of ΔH_a reflecting the endothermic nature of the dissolution process of MS in 1 M HCl, and their values in presence of **4-CP** and **DPP** are higher than those obtained for the blank electrolyte [65]. It is possible to distinguish between the chemisorption and the physisorption process basing on the absolute value of ΔH_a, For a physisorption adsorption the enthalpy is equal to or lower than 40 kJ mol^{-1} while, a chemisorption it is equal to or higher than 100 kJ mol^{-1} [66]. In our case the calculated values of ΔH_a for **4-CP** and **DPP** are higher than 40 but lower than 100 kJ mol^{-1} suggest that their mode of adsorption on the metal surface is combination of chemisorption and physisorption. The increase of ΔS_{ac} value in the inhibited media compared to the uninhibited which implies that a rise in the disordering of the inhibited electrolyte.

3.4. Adsorption consideration

Herein, the surface coverage (θ) data were obtained from EIS measurements, corresponding to different inhibitor concentrations in 1 M HCl at 298 K and got by the following eq.:

$$\theta = \frac{\eta_{EIS}}{100} \tag{8}$$

Where η_{EIS} is the inhibition efficiency of the inhibitor.

In order to trace the best-fit adsorption isotherm, the degree of surface coverage and concentration of the inhibitor are essential. Thereby, trials were applied to fit this data for various isotherms that are the Langmuir isotherm (θ / 1 - θ) = K_{ads} C_{inh}), Temkin isotherm, Frumkin isotherm, and Freundlich isotherm, out of these trials, Langmuir adsorption isotherm suited in the best way. According to Langmuir isotherm [67], θ is associated with C_{inh} as:

$$\frac{C_{inh}}{\theta} = \frac{1}{K_{ads}} + C_{inh} \tag{9}$$

Where θ is referred to as the degree of surface coverage, K_{ads} is termed as the equilibrium constant for the adsorption phenomenon, and C_{inh} represents the concentration of the present 4-CP and DPP inhibitors. The plot between C_{inh}/θ and C_{inh} resulted in a straight line evidencing about obey of Langmuir kind of adsorption for most of the concentration cases of the 4-CP and DPP with uniform monolayer formation (Fig. 7). The obtained curves generally form straight lines with regression factors close to 1. K_{ads} can be computed via an intercept i.e. eq. (9) and Table 6 (the values indicate physiochemical mode of surface adsorption) and hence, Free energy of adsorption can be obtained using this K_{ads} as shown in eq. (10).

$$K_{ads} = \frac{1}{55.5}\exp\left(\frac{-\Delta G^{\circ}_{ads}}{RT}\right) \tag{10}$$

The value of adsorption equilibrium constant K_{ads} is related to standard Gibb's free energy by [68]:

$$\Delta G^{\circ}_{ads} = -RTLn(55.5\,K_{ads}) \tag{11}$$

where 55.5 is the molar concentration of H_2O, R(universal gas constant) and T as the absolute temperature (Kelvin).

Table 5
Values of activation parameters for the dissolution of MS in 1 M HCl with and without addition of **4-CP** and **DPP**.

Medium	E_a (kJ mol^{-1})	ΔH_a (kJ mol^{-1})	ΔS_a (J mol^{-1} K^{-1})
1 M HCl	49.27	46.59	−95.98
10^{-3} M of **DPP**	70.46	67.78	−36.27
10^{-3} M of **4-CP**	89.61	86.93	16.89

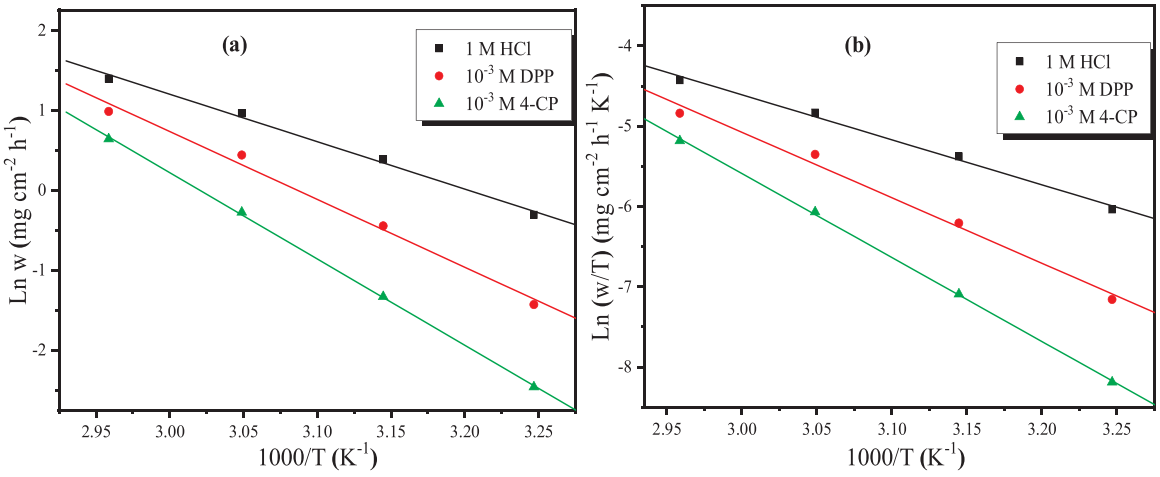

Fig. 6. (a) Arrhenius and (b) Transition Arrhenius plots of MS in 1 M HCl containing **4-CP** and **DPP**.

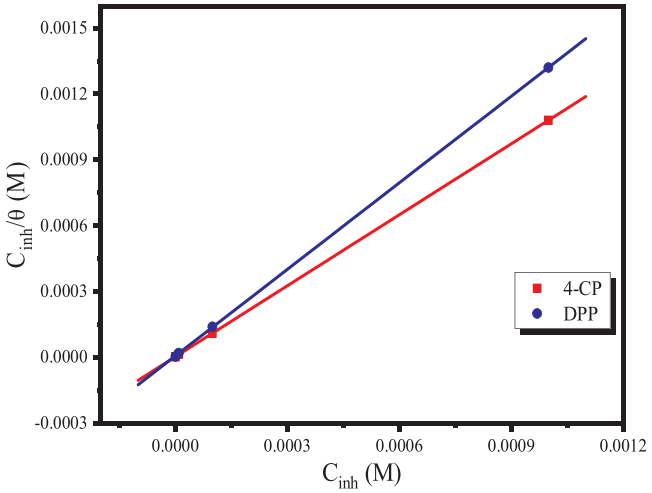

Fig. 7. Langmuir adsorption curves for MS in the acidic electrolyte with various doses of **4-CP** and **DPP**.

Table 6
Thermodynamic parameters of adsorption for **4-CP** and **DPP** on the MS in acidic media.

Medium	R^2	K_{ads} (M^{-1})	ΔG°_{ads} (kJ $mole^{-1}$)
DPP	0.9999	2.0204×10^5	−40.22
4-CP	1.0000	6.6517×10^5	−43.16

Generally, a wide value of K_{ads} suggests that the inhibitor is strongly and easily adsorbed on the metal surface resulting in better protection efficiencies. In this case, the strong interaction of inhibitors with MS can be attributed to the presence of heteroatoms, such as *O* and *N*, and π -electrons in the inhibitor molecules. As seen in Table 6, the value of K_{ads} follow **4-CP** > **DPP** indicates that the **4-CP** exhibits stronger adsorption stability than **DPP**. The adsorption energies of two inhibitors (**4-CP** and **DPP**) are less -40 KJ/mol. This result shows that the two inhibitors (**4-CP** and **DPP**) are adsorbed on the metal surface by chemical bonds (chemisorption) [62].

3.5. Surface examination

The surface morphology of MS coupon surface after and before immersion in uninhibited and inhibited solutions are illustrated in Fig. 8. No apparent defects are shown in SEM image of abraded metal surface just polishing scratches are noticed. SEM image that was taken after immersion in 1 M HCl for 06 h shows a formed rust layer with fine plates structure (flowery structure) covering all the appeared metal surface. After immersion in inhibited acidic solution by 10^{-3} M of the **4-CP** and **DPP** inhibitors, a smooth surface is observed with some polishing scratches. Which indicates that the reduction in corrosion rate is caused by forming of a protective layer on the MS surface.

3.6. DFTs, Monte Carlo (MC) and MD simulations

3.6.1. DFT results

The highest occupied molecular orbital (HOMO) and the lowest unoccupied molecular orbital (LUMO) shape and symmetry have proven as important parameters for evaluating the reactivity of a

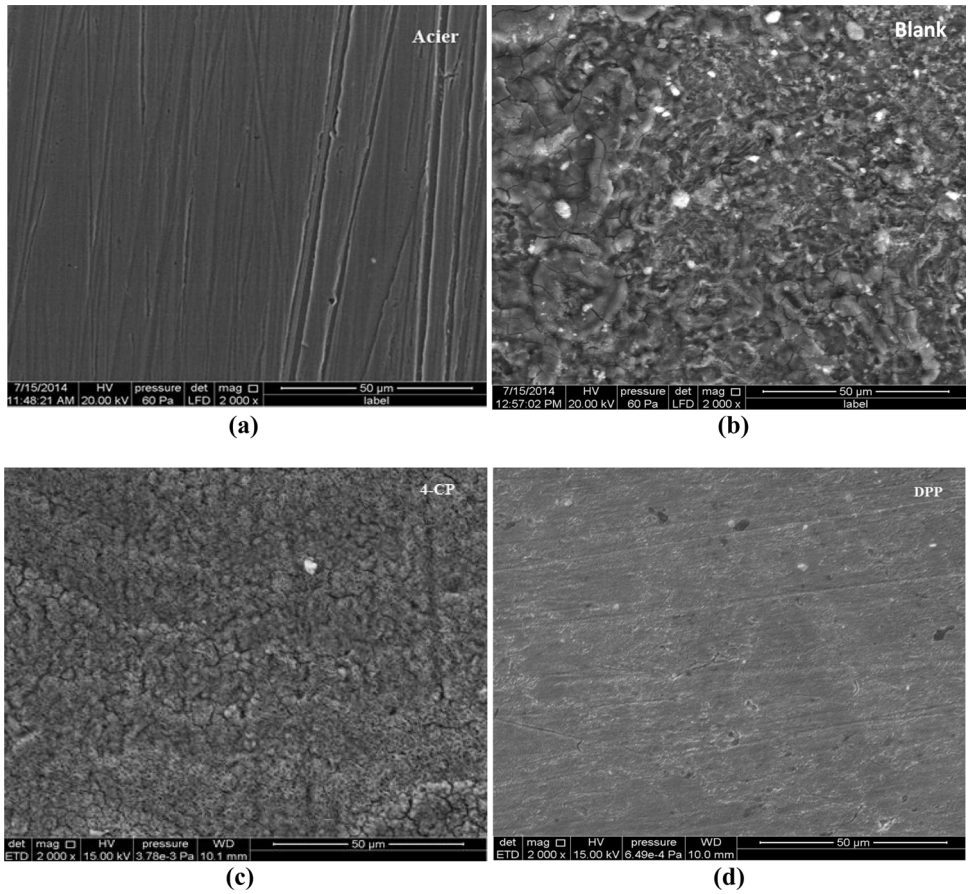

Fig. 8. SEM micrographs of mild steel surface: a) Metallic surface after being polished, b) metallic surface after immersion in 1 M HCl and c) metallic surface after immersion in 1 M HCl with 10^{-3} M **4-CP**, d) metallic surface after immersion in 1 M HCl with 10^{-3} M **DPP** at 298 K with Scale =50 µm.

molecule as well as estimating the course of chemical reactions [69]. The HOMO depicts the regions of the molecule that have a predisposition to donate electrons to electrophilic species while the LUMO points out to the regions of the molecule with a high tendency to accept electrons from nucleophilic species.

The highest occupied molecular orbital (HOMO), the lowest unoccupied molecular orbital (LUMO), Moelcular Orbitals (OM) and the molecular electrostatic potential (MEP) of the **DPP** and **4-CP** are presented in Fig. 9 and numerous DFT indices are given in Table 7. The frontier molecular orbitals (MO's) picture revealed that in the **DPP** molecule HOMO is primarily distributed over the phenyl ring, the central -N-*N*-H – C═O bond linking (acetohydrazide group) and minor distribution on the side of the pyrazole ring. The same holds true for the **4-CP** molecule.

The LUMO distribution has some differences in the region of phenyl ring. The relatively high values of HOMO for both **4-CP** and **DPP** molecules point out toward their ability to for the interaction with the iron surface through electron-donation and acceptation as well [70]. Based on the increasing E_{HOMO} values, the order of change in inhibitory efficiencies of our compounds is consistent with the order obtained from the experimental results (**4-CP** and **DPP**). This is supported by their low electron affinity and high ionization potential values, thus confirming the equivalent order of electron exchange aptitude. Similarly, relatively high value of chemical softness and low value of hardness are also expected values supporting that both of the inhibitor molecules (**DPP** and **4-CP**) are highly reactive species and possess the adsorptive tendency when they are in the vicinity of the metal surfaces. For both of the inhibitors the value of the Fraction of transferred electrons (ΔN) (-0.276 for **DPP** and -0.3092 for **4-CP**) expresses the strong ability of these inhibitors for electron donation to the metal surface.

Table 7
Calculated theoretical chemical parameters for **DPP** and **4-CP** and the corresponding equations used for their calculation.

Theoretical parameters	DPP	4-CP
E_{HOMO} (eV)	−6.0160	−5.9990
E_{LUMO} (eV)	−2.4300	−2.5770
Ionization energy (I)	6.0408	6.0408
Electron affinity (A)	6.0160	5.9990
Electronegativity (χ)	4.2230	4.2880
Global hardness (η)	1.7930	1.7110
Chemical potential (π)	−4.2230	−4.2880
Global softness (σ)	0.5577	0.5845
Global electrophilicity (ω)	4.9732	5.3732
Electrodonating (ω-) power	7.3088	7.7310
Electroappcepting (ω+) power	3.0858	3.4430
Net electrophilicity (Δω+-)	2.9490	3.3137
Fraction of transferred electrons (ΔN)	−0.2769	−0.3092
Energy from Inhb to Metals (ΔN)	0.1375	0.1636
ΔE back-donation	−0.4483	−0.4278

Equations used in the calculations: $\Delta E = E_{LUMO}-E_{HOMO}$, $I = -E_{HOMO}$, $A = -E_{LUMO}$, $\chi = 0.5(I + A)$, $\eta = 0.5(I-A)$, $S = 1/\eta$, $\omega = \chi^2/2\eta$, $\varepsilon = 1/\omega$, $\Delta N_{110} = (4.82-\chi_{inh})/2(\eta_{inh}+\eta_{Fe})$, $\Delta\psi = (\chi_{Fe}-\chi_{inh})^2/4(\eta_{Fe}+\eta_{inh})$, $\Delta E_{d\text{-}b} = -\eta/4$.

MAC are proven very useful for indicating the responsible sites (atoms) of the inhibitors that are accountable for the adsorption onto the metals. The interaction between Fe(110) and the inhibitor molecules is often considered to preferentially take place on the atom with the highest negative charge [71,72]. The MAC for the **DPP** and **4-CP** are presented in Fig. 10 the highest negative charge on both of the inhibitor

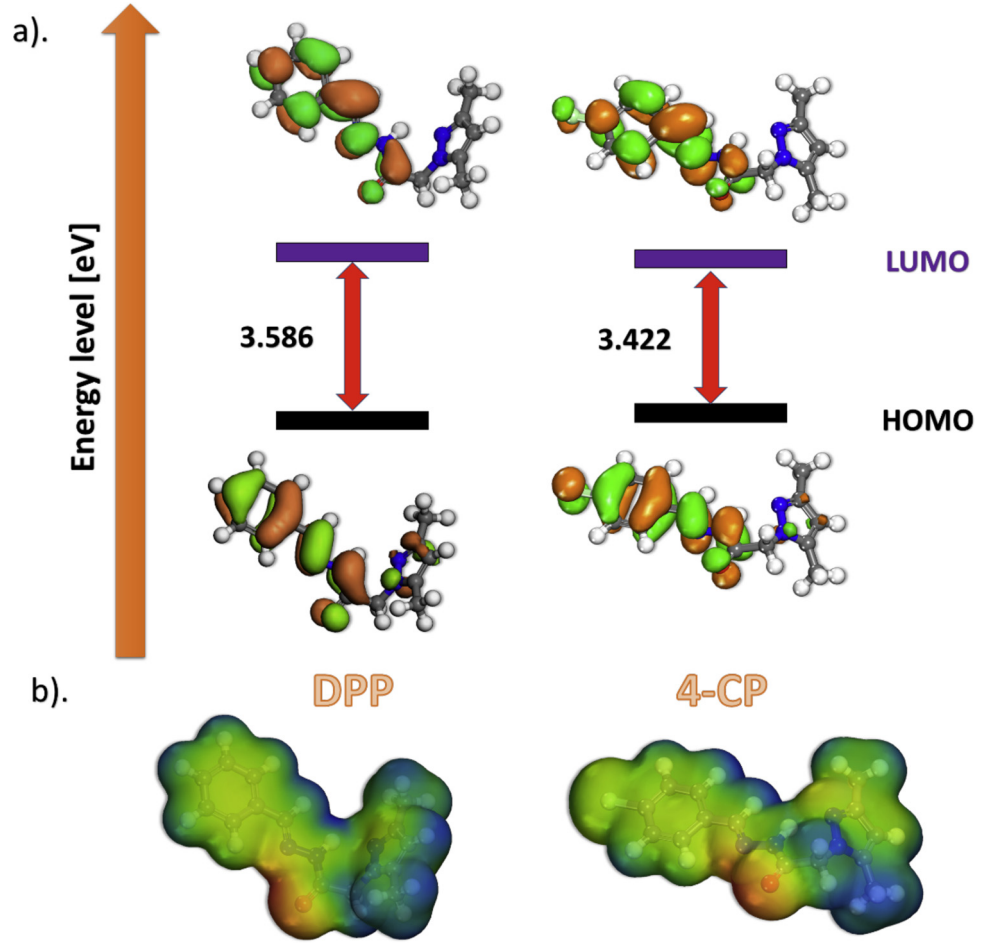

Fig. 9. Optimized structure, HOMO, LUMO surfaces, and molecular electrostatic potential (MEP) of **DPP** and **4-CP**.

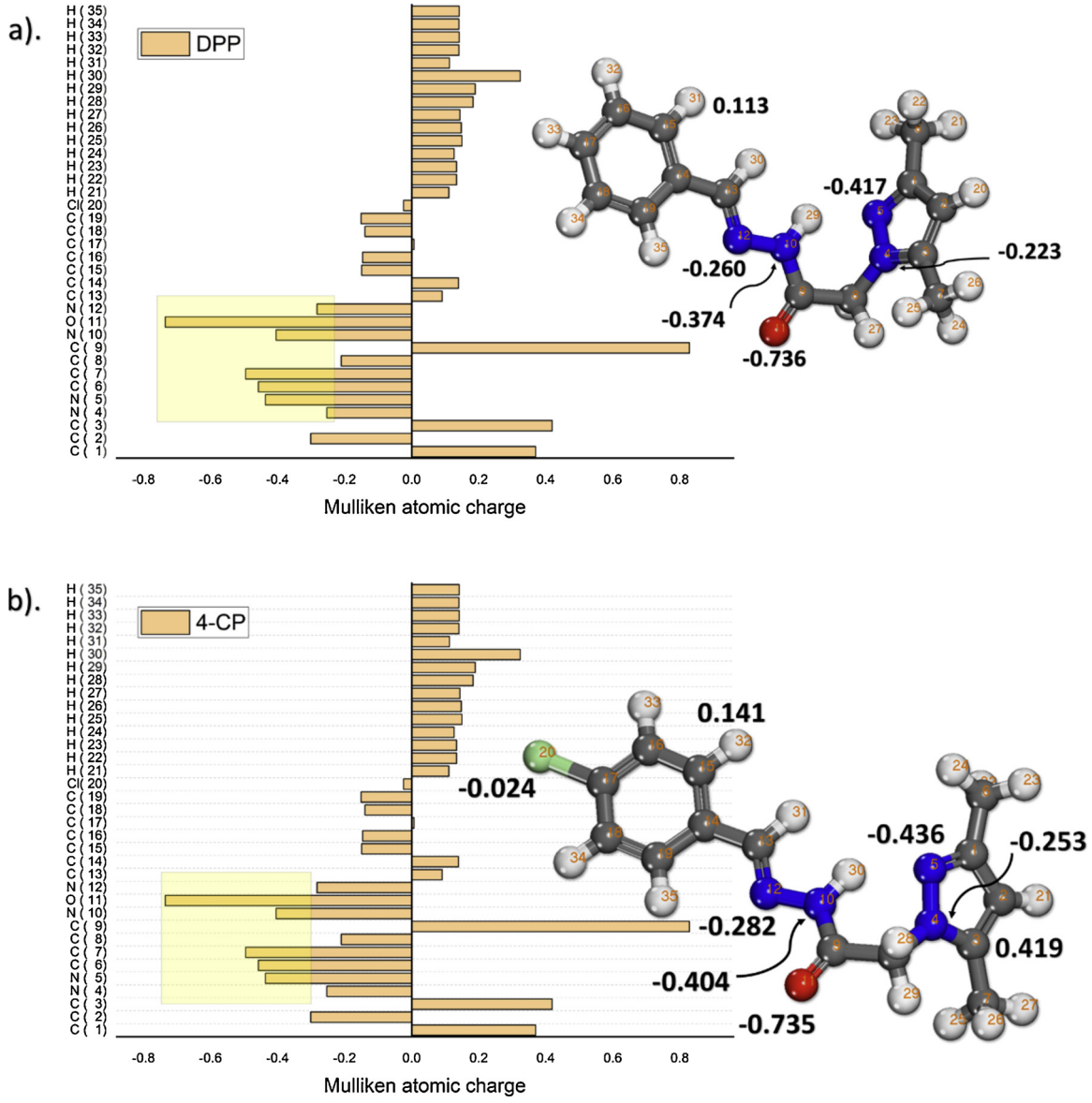

Fig. 10. DPP and **4-CP** structures and their Mulliken atomic charges (MAC) - the most favorable centers are depicted in the figures using the yellow square (For interpretation of the references to colour in this figure legend, the reader is referred to the web version of this article).

molecules are located on: O and N, implying on that these centers have the highest electron density and would favorably interact with the Fe (110). This is observable also in Fig. 9 were is presented the molecular electrostatic potential (MEP) for the molecules.

3.6.2. Monte Carlo and molecular dynamic simulations

In the Fig. 11 are presented the lowest energy configurations of **DPP** and **4-CP** inhibitors on the Fe (110) surface in the simulated corrosion media (230 H_2O molecules + 15 H_3O^+ and 15 Cl^- ion system). The adsorption geometries of the inhibitors (as suggested by Mulliken charges) imply that this process is supported through oxygen and nitrogen atoms. This adsorption behavior leads toward the creation of an anti-corrosion layer onto the Fe(110) surface that protects the metal [72].

The quantitative evaluation of the interaction between inhibitor molecules (**DPP** or **4-CP**) with the Fe (110) surface, is performed through calculation of the adsorption energies using the following equation:

$$E_{ads} = E_{total} - [E_{surface+water} + E_{(DPP\ or\ 4-CP)+surface}] + E_{water} \quad (12)$$

where: E_{total} is the total energy of the system as a result of inhibitor-metal interaction; $E_{surface\ +\ water}$ and $E_{(DPP\ or\ 4\text{-}CP)+\ water}$ is system energy in the absence and presence of **DPP** or **4-CP** molecules.

The distribution of the adsorption energies for the huge number of adsorptive configurations generated and calculated by MC for the inhibitors is shown in Fig. 12. The E_{ads} value for the adsorption of **4-CP** is at some extent higher ($E_{ads/4\text{-}CP}$ = -109.18 kcal/mol) than that of **DPP** inhibitor ($E_{ads/DPP}$ = -103.38 kcal/mol) on Fe (110). The higher $E_{ads}$for the **4-CP** molecule in rapport of the **DPP** is in full agreement with experimental results and indicates a strong interaction of the inhibitors onto the iron surface – leading to efficient corrosion protection of iron.

MD simulations are effective as there are able to follow and capture the dynamics of the adsorption of the studied inhibitors on the Fe(110) surface. In the Fig. 13 shows last configurations of **DPP** and **4-CP** on Fe (110) in the simulated corrosion media [(**DPP** or **4-CP**) /15 hydronium + 15 chloride ions].

From the Fig. 13, it's evident that both of the inhibitors adsorb effectively on the Fe (110) surface. From the figure of the adsorbed inhibitors it is apparent that both of the molecules are oriented toward the iron surface in the position that allows them a maximum contact on

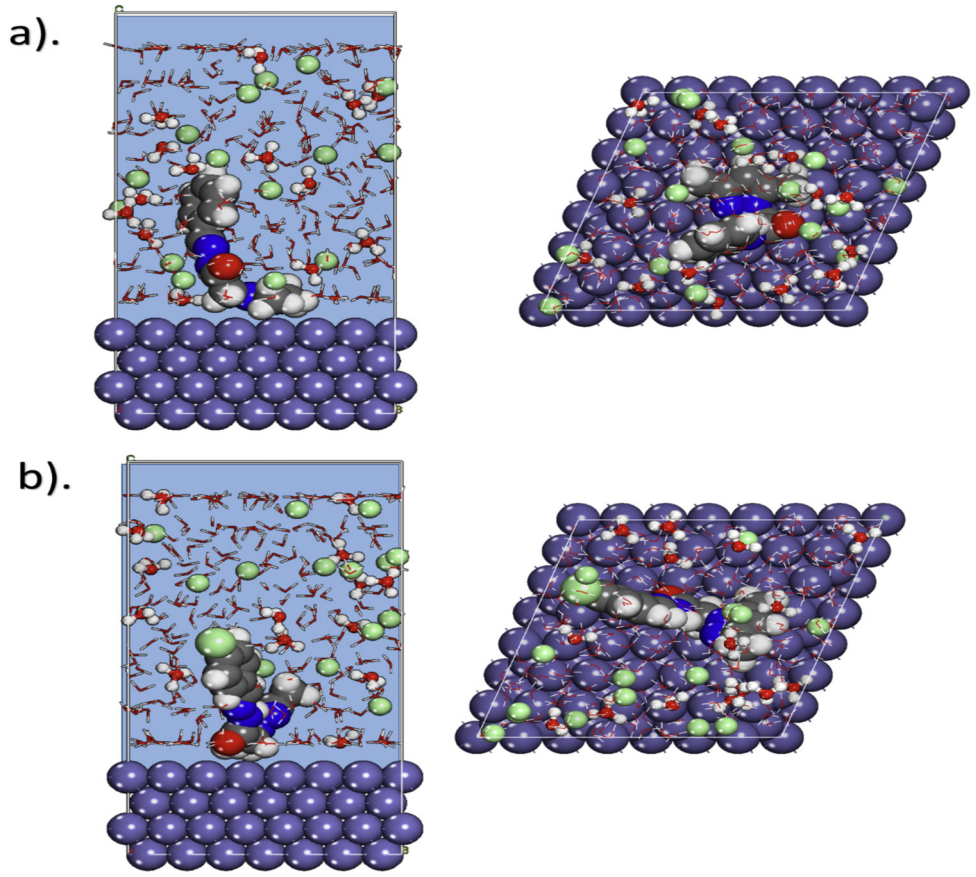

Fig. 11. MC poses of the lowest adsorption configurations for the: a. **DPP** and b. **4-CP** inhibitors in the simulated corrosion media on the Fe (1 1 0) substrate.

the O and nitrogen atoms (as suggested by Mulliken charges). This conclusion is supported also by the analysis of the Radial Distribution Function (RDF) calculated for O, N and Cl (for **4-CP**) atoms from the plane of the Fe(110) surface presented in the Fig. 14. The radial distribution function (RDF) has proven as a useful mean to evaluate the interaction of inhibitors with the surface [70].

In general, when the peak appears in the RDF graph of particular atom(s) and the surface in the range from 1 and 3.5 Å it corresponds to chemisorption, while in the case of physisorption the appereance of the RDF peaks is expected at larger distances from the surface plan of metal (usually greater than 3.5 Å). The RDF of the heteroatoms (N and O) for the studied inhibitors is at smaller range than 3.5 Å. The results

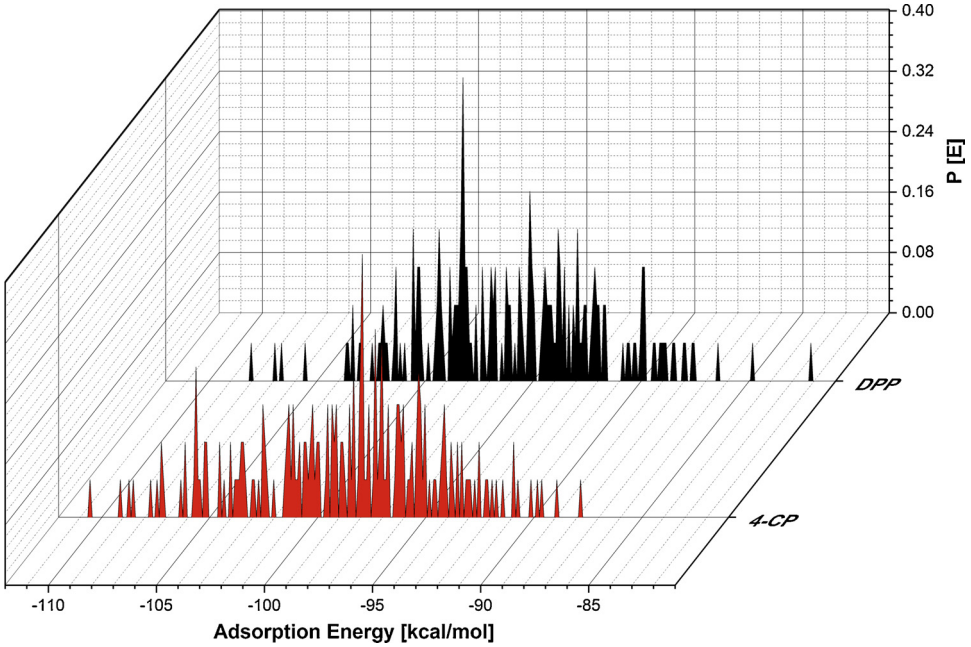

Fig. 12. Distribution of adsorption energies for **DPP** and **4-CP** obtained via MC.

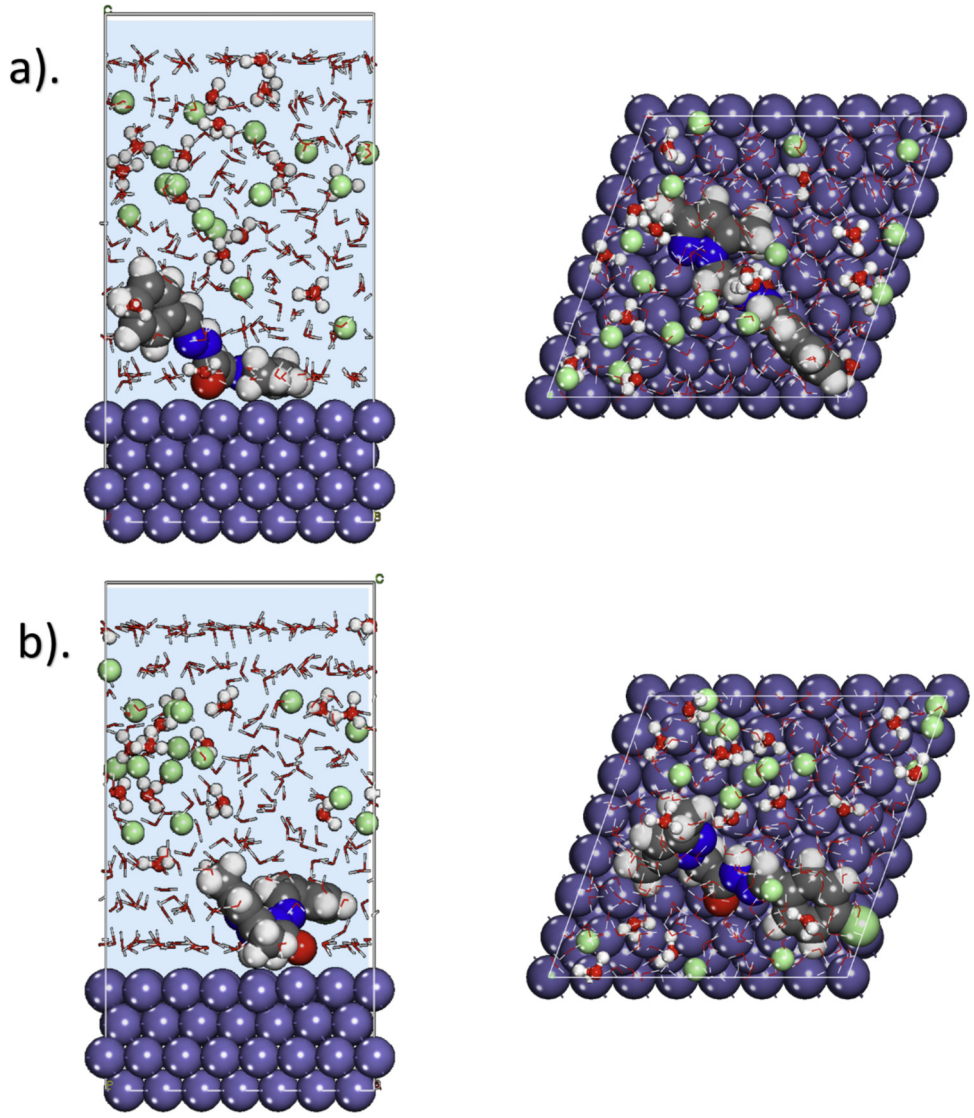

Fig. 13. Lowest energy adsorption configurations for the: a. **DPP** and b. **4-CP** inhibitors in the simulated corrosion media on the Fe (1 1 0) substrate obtained by MD simulations.

obtained from MD and corresponding RDF analysis confirm once more (in line with experimental results and MC calculations) the strong tendency of the inhibitors to adsorb and protect the metal, due to its greater tendency to provide and receive electrons to the metal surface [70,73].

3.7. Mechanism of inhibition

The mechanism of inhibition action can be explained on the basis of mode of adsorption. Adsorption is influenced by the chemical structure of **DPP** and **4-CP**, its nature and surface charge, the distribution of charge in the molecule. In general, the charge on the metal surface, type of interaction with the metal surface, and chemical structure of inhibitor influence the adsorption phenomenon. **DPP** and **4-CP** have electronegative donor atoms N, O and π electrons of the aromatic ring. These electronegative donor atoms or π electrons of the aromatic ring or both of them cause efficient adsorption of inhibitors onto the MS surface. These electron rich centers transfer their non-bonding and π-electrons into surface metallic orbital and form coordination bondings [74,75]. Hence the protonated inhibitors have a tendency to adsorb onto the metal surface through electrostatic interaction between the positively charged molecules and the negatively charged metal surface, thus facilitating physical adsorption of the inhibitor. This adsorption on the surface results in formation of a protective film which displace water from the metal surface and protect it against corrosion.

4. Conclusion

The investigation carried out on MS in a solution of 1 M HCl in the presence of two new pyrazol derivatives has established by various techniques and methods. Both **4-CP** and **DPP** demonstrate a phenomenal protective capacity for the corrosion of MS in 1 M HCl at 298 K, and the inhibition efficiencies of **4-CP** and **DPP** decrease in the order of **4-CP** > **DPP** at all concentrations. **4-CP** and **DPP** behaved as mixed-type corrosion inhibitors. One-half circle, relating to just one time constant, is seen in the Nyquist plots with the addition of **4-CP** and **DPP**, the outcomes acquired from EIS, Tafel polarization and gravimetric measurements have a reasonable degree of consistency. The adsorption of the **4-CP** and **DPP** on MS in 1 M HCl pursues the Langmuir isotherm and the corresponding thermodynamic parameters suggested that the **4-CP** and **DPP** chemisorbed on MS surface by training a protective barrier which is affirmed by SEM examination. DFT calculations were able the pin-point the adsorption centers of the inhibitors. Moreover, the MC and MD calculations are supportive of the strong

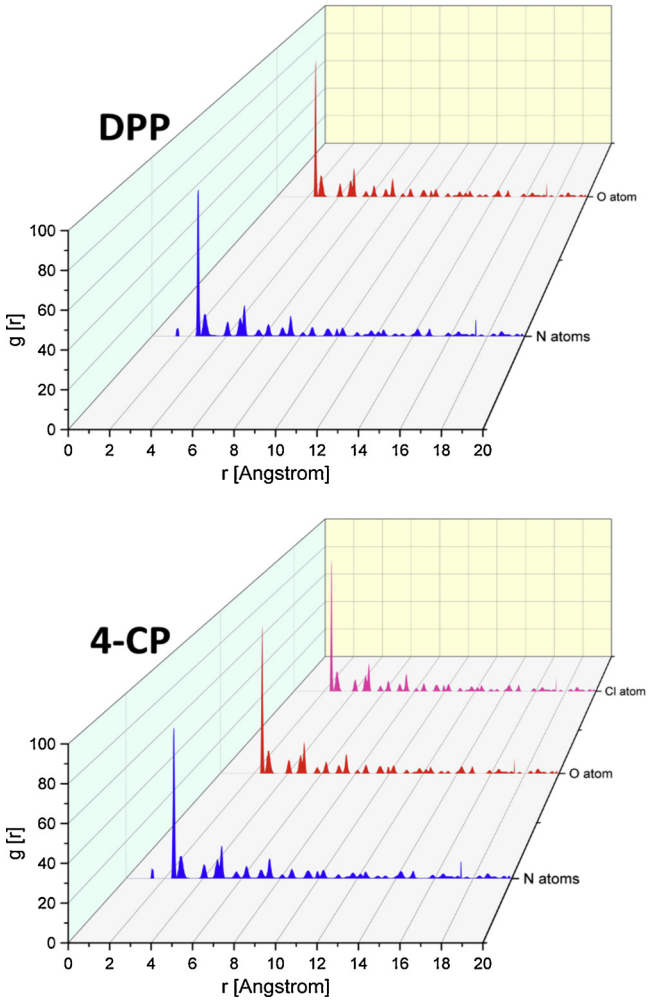

Fig. 14. RDF of heteroatoms for: a. **DPP** and b. **4-CP** inhibitors on the Fe (111) surface obtained from the analysis of MD trajectory.

adsorption interaction of **DPP** and **4-CP** towards the iron surface, giving molecular details regarding the adsorption behavior (geometry) and the adsorption energy of these species onto the iron surface. The presented theoretical results (DFT, MC and MD) are in full agreement with the experimental ones.

CRediT authorship contribution statement

Siham El Arrouji: Data curation, Investigation, Methodology, Visualization. **Khalid Karrouchi:** Visualization, Writing - original draft, Writing - review & editing. **Avni Berisha:** Visualization, Formal analysis, Writing - original draft, Writing - review & editing. **Khadija Ismaily Alaoui:** Resources. **Ismail Warad:** Resources. **Zakia Rais:** Conceptualization, Methodology, Project administration, Supervision, Resources. **Smaail Radi:** Supervision, Investigation. **Mustapha Taleb:** Conceptualization, Methodology, Project administration, Supervision, Resources. **M'hammed Ansar:** Supervision, Resources. **Abdelkader Zarrouk:** Writing - original draft, Writing - review & editing.

Declaration of Competing Interest

The authors declare that they have no known competing financial interests or personal relationships that could have appeared to influence the work reported in this paper.

Acknowledgments

This research was partially supported by University Sidi Mohamed Ben Abdellah-Fez and UM5R. Avni Berisha gratefully acknowledges the support from the Ministry of Education, Science and Technology of Kosovo (Nr.2-5069) for providing the computing resources.

Appendix A. Supplementary data

Supplementary material related to this article can be found, in the online version, at doi:https://doi.org/10.1016/j.colsurfa.2020.125325.

References

[1] G. Schmitt, Application of inhibitors for acid media: report prepared for the european federation of corrosion working party on inhibitors, Br. Corros. J 19 (1984) 165–176.
[2] A. Zarrouk, H. Zarrok, Y. Ramli, M. Bouachrine, B. Hammouti, A. Sahibed-dine, F. Bentiss, Inhibitive properties, adsorption and theoretical study of 3,7-dimethyl-1-(prop-2-yn-1-yl)quinoxalin-2(1H)-one as efficient corrosion inhibitor for carbon steel in hydrochloric acid solution, J. Mol. Liq. 222 (2016) 239–252.
[3] M. El Hezzat, M. Assouag, H. Zarrok, Z. Benzekri, A. El Assyry, S. Boukhris, A. Souizi, M. Galai, R. Touir, M. Ebn Touhami, H. Oudda, A. Zarrouk, Correlated DFT and electrochemical study on inhibition behavior of ethyl 6-amino-5-cyano-2-methyl-4-(p-tolyl)-4H-pyran-3-carboxylate for the corrosion of mild steel in HCl, Der Pharma Chem. 7 (10) (2015) 77–88.
[4] M. El Faydy, M. Galai, A. El Assyry, A. Tazouti, R. Touir, B. Lakhrissi, M. Ebn Touhami, A. Zarrouk, Experimental investigation on the corrosion inhibition of carbon steel by 5-(chloromethyl)-8-quinolinol hydrochloride in hydrochloric acid solution, J. Mol. Liq. 219 (2016) 396–404.
[5] M.M. Solomon, S.A. Umoren, In-situ preparation, characterization and anticorrosion property of polypropylene glycol/silver nanoparticles composite for mild steel corrosion in acid solution, J. Colloid Interface Sci. 462 (2016) 29–41.
[6] M. Talari, S.M. Nezhad, S.J. Alavi, M. Mohtashamipour, A. Davoodi, S. Hosseinpour, Experimental and computational chemistry studies of two imidazole-based compounds as corrosion inhibitors for mild steel in HCl solution, J. Mol. Liq. 286 (2019) 110915.
[7] P. Arellanes-Lozada, O. Olivares-Xometl, N.V. Likhanova, I.V. Lijanova, J.R. Vargas-García, R.E. Hernández-Ramírez, Adsorption and performance of ammonium-based ionic liquids as corrosion inhibitors of steel, J. Mol. Liq. 265 (2018) 151–163.
[8] M. Jokar, T.S. Farahani, B. Ramezanzadeh, Electrochemical and surface characterizations of morus alba pendula leaves extract (MAPLE) as a green corrosion inhibitor for steel in 1 M HCl, J. Taiwan Inst. Chem. Eng. 63 (2016) 436–452.
[9] H. Zarrok, S.S. Al-Deyab, A. Zarrouk, R. Salghi, B. Hammouti, H. Oudda, M. Bouachrine, F. Bentiss, Thermodynamic characterisation and Density Functional Theory Investigation of 1, 1',5, 5'-Tetramethyl-1H, 1'H-3, 3'- bipyrazole as Corrosion Inhibitor of C38 Steel Corrosion in HCl, Int. J. Electrochem. Sci. 7 (2012) 4047–4063.
[10] M.E. Faydy, M. Rbaa, L. Lakhrissi, B. Lakhrissi, I. Warad, A. Zarrouk, I.B. Obot, Corrosion protection of carbon steel by two newly synthesized benzimidazol-2-ones substituted 8-hydroxyquinoline derivatives in 1 M HCl: Experimental and theoretical study, J. Surf. Interfaces Mater. 14 (2019) 222–237.
[11] M. Alfakeer, M. Abdallah, A. Fawzy, Corrosion inhibition effect of expired ampicillin and flucloxacillin drugs for mild steel in aqueous acidic medium, Int. J. Electrochem. Sci. 15 (2020) 3283–3297.
[12] R.S. Abdel Hameeda, M. Abdallah, Corrosion inhibition of carbon steel in 1 m hydrochloric acid using some pyrazolo[3,4-d]Pyrimidnone derivatives, Prot. Met. Phys. Chem. Surf. 54 (1) (2018) 113–121.
[13] M. Abdallah, H.E. Meghed, M. Sobhi, Inhibiting effect of Ni2+ cation + 3-methyl pyrazolone as a corrosion inhibitor for carbon steel in sulfuric acid solution, Mater. Chem. Phys. 118 (2009) 111–117.
[14] D. Ben Hmamou, R. Salghi, A. Zarrouk, H. Zarrok, S.S. Al-Deyab, O. Benali, B. Hammouti, The inhibited effect of phenolphthalein towards the corrosion of C38 steel in hydrochloric acid, Int. J. Electrochem. Sci. 7 (2012) 8988–9003.
[15] D. Ben Hmamou, R. Salghi, A. Zarrouk, H. Zarrok, B. Hammouti, S.S. Al-Deyab, M. Bouachrine, A. Chakir, M. Zougagh, Alizarin red: an efficient inhibitor of C38 steel corrosion in hydrochloric acid, Int. J. Electrochem. Sci. 7 (2012) 5716–5733.
[16] H. Zarrok, K. Al Mamari, A. Zarrouk, R. Salghi, B. Hammouti, S.S. Al-Deyab, E.M. Essassi, F. Bentiss, H. Oudda, Gravimetric and electrochemical evaluation of 1-allyl-1Hindole-2,3-dione of carbon steel corrosion in hydrochloric acid, Int. J. Electrochem. Sci. 7 (2012) 10338–10357.
[17] A. Zarrouk, M. Messali, M.R. Aouad, M. Assouag, H. Zarrok, R. Salghi, B. Hammouti, A. Chetouani, Some new ionic liquids derivatives: synthesis, characterization and comparative study towards corrosion of C-steel in acidic media, J. Chem. Pharm. Res. 4 (7) (2012) 3427–3436.
[18] I. Bouabdallah, L.A. M'Barek, A. Zyad, A. Ramdani, I. Zidane, A. Melhaoui, New pyrazolic compounds as cytotoxic agents, Nat. Prod. Res. 21 (4) (2007) 298–302.
[19] K. Karrouchi, L. Chemlal, J. Taoufik, Y. Cherrah, S. Radi, M. El Abbes, M.Ansar Faouzi, Synthesis, antioxidant and analgesic activities of Schiff bases of 4-amino-1,2,4-triazole derivatives containing a pyrazole moiety, Ann. Pharm. Fr. 74 (2016) 431–438.

[20] M.S. Christodoulou, S. Liekens, K.M. Kasiotis, S.A. Haroutounian, Novel pyrazole derivatives: synthesis and evaluation of anti-angiogenic activity, Bioorg. Med. Chem. 18 (12) (2010) 4338–4350.

[21] K. Karrouchi, E. Yousfi, N. Sebbar, Y. Ramli, J. Taoufik, Y. Ouzidan, M. Ansar, Y.N. Mabkhot, H.A. Ghabbour, S. Radi, New pyrazole-hydrazone derivatives: X-ray analysis, molecular structure investigation via density functional theory (DFT) and their high in-situ catecholase activity, . Inter. J. Mol. Sci. 18 (2017) 2215.

[22] M.J. Ahsan, J.G. Samy, K.R. Dutt, U.K. Agrawal, B.S. Yadav, S. Vyas, R. Kaur, G. Yadav, Design, synthesis and antimycobacterial evaluation of novel 3-substituted-N-aryl6,7-dimethoxy-3a,4-dihydro-3H-indeno[1,2-c] pyrazole-2- carboxamide analogues, Bioorg. Med. Chem. Lett. 21 (15) (2011) 4451–4453.

[23] K. Karrouchi, S. Radi, Y. Ramli, J. Taoufik, Y. Mabkhot, F. Al-aizari, M. ansar, Synthesis and pharmacological activities of pyrazole derivatives: a review, Molecules 23 (2018) 134.

[24] M.J. Ahsan, H. Khalilullah, J.P. Stables, J. Govindasamy, Synthesis and anticonvulsant activity of 3a, 4-dihydro-3Hindeno[1, 2-c]pyrazole-2-carboxamide/ carbothioamide analogues, J. Enzyme Inhib. Med. Chem. 28 (3) (2013) 644–650.

[25] R.R. Pillai, K. Karrouchi, S. Fettach, S. Armaković, S.J. Armaković, Y. Brik, J. Taoufik, S. Radi, M.E.A. Faouzi, M.H. Ansar, Synthesis, spectroscopic characterization, reactive properties by DFT calculations, molecular dynamics simulations and biological evaluation of Schiff bases tethered 1, 2, 4-triazole and pyrazole rings, J. Mol. Struct. 1177 (2019) 47–54.

[26] H. Khalilullah, S. Khan, M.J. Ahsan, B. Ahmed, Synthesis and antihepatotoxic activity of 5-(2,3-dihydro1,4-benzodioxane-6-yl)-3-substituted-phenyl-4,5-dihydro-1Hpyrazole derivatives, Bioorg. Med. Chem. Lett. 21 (24) (2011) 7251–7254.

[27] M.J. Alam, M.J. Ahsan, O. Alam, S.A. Khan, Synthesis of 4-(5-chloro-3-methyl-1-phenyl-1H-pyrazol-4-yl)- 6-(substituted phenyl)pyrimidin-2-ol analogues as 8 antiinflammatory and analgesic agents, Lett. Drug Des. Discovery 10 (8) (2013) 776–782.

[28] K. Karrouchi, S. Fettach, S. Radi, J. Taoufik, Y.N. Mabkhot, S. Alterary, My E.A. Faouzi, M. Ansar, Synthesis, Characterization, Free-radical scavenging Capacity and Antioxidant Activity of Novel Series of Hydrazone, 1, 3, 4-oxadiazole and 1, 2, 4-triazole derived from 3, 5-dimethyl-1H-pyrazole, Lett. Drug Des. Discov. 16 (2019) 712–720.

[29] A. Khadraoui, A. Khelifa, M. Hadjmeliani, R. Mehdaoui, K. Hachama, A. Tidu, Z. Azari, I.B. Obot, A. Zarrouk, Extraction, characterization and anti-corrosion activity of Mentha pulegium oil: weight loss, electrochemical, thermodynamic and surface studies, J. Mol. Liq. 216 (2016) 724–731.

[30] Y. ELouadi, F. Abrigach, A. Bouyanzer, R. Touzani, O. Riant, B. ElMahi, A. El Assyry, S. Radi, A. Zarrouk, B. Hammouti, Corrosion inhibition of mild steel by new N-heterocyclic compound in 1 M HCl: experimental and computational study, Der Pharma Chem. 7 (8) (2015) 265–275.

[31] R. Peverati, D.G. Truhlar, M11-L: A Local Density Functional That Provides Improved Accuracy for Electronic Structure Calculations in Chemistry and Physics, J. Phys. Chem. Lett. 3 (1) (2012) 117–124.

[32] J.P. Perdew, K. Burke, M. Ernzerhof, Generalized gradient approximation made simple, Phys. Rev. Lett. vol. 77 (1996) 3865–3868.

[33] A. Berisha, C. Combellas, F. Kanoufi, P. Decorse, N. Oturan, J. Médard, M. Seydou, F. Maurel, J. Pinson, Some theoretical and experimental insights on the mechanistic routes leading to the spontaneous grafting of gold surfaces by diazonium salts, Langmuir 33 (2017) 8730–8738.

[34] A. Klamt, The COSMO and COSMO-RS solvation models, wiley interdiscip, Rev. Comput. Mol. Sci. 8 (2017) e1338.

[35] A.S. Lemak, N.K. Balabaev, On the berendsen thermostat, Mol. Simul. 13 (3) (1994) 177–187.

[36] H. Sun, Z. Jin, C. Yang, R.L. Akkermans, S.H. Robertson, N.A. Spenley, S. Miller, S.M. Todd, COMPASS II: extended coverage for polymer and drug-like molecule databases, J. Mol. Model. 22 (2) (2016) 47, https://doi.org/10.1007/s00894-016-2909-0.

[37] V.V. Mehmeti, A.R. Berisha, Corrosion study of mild steel in aqueous sulfuric acid solution using 4-Methyl-4H-1, 2, 4-Triazole-3-Thiol and 2-Mercaptonicotinic acid—an experimental and theoretical study, Front. Chem. 5 (2017) 61 doi.org/10.3389/fchem.2017.00061.

[38] O. Dagdag, A. Berisha, Z. Safi, O. Hamed, S. Jodeh, C. Verma, A. El Harfi, DGEBA-polyaminoamide as effective anticorrosive material for 15CDV6 steel in NaCl medium: computational and experimental studies, J. Appl. Polym. Sci. 137 (8) (2020) 48402.

[39] A. Ghazoui, N. Benchat, F. El Hajjaji, M. Taleb, Z. Rais, R. Saddik, A. Elaatiaoui, B. Hammouti, The study of the effect of ethyl (6-methyl-3-oxopyridazin-2-yl) acetate on mild steel corrosion in 1M HCl, J. Alloys. Compd. 693 (2017) 510–517.

[40] J. Saranya, F. Benhiba, N. Anusuya, Ram Subbiah, A. Zarrouk, S. Chitra, Experimental and computational approaches on the pyran derivatives for acid corrosion, Colloids Surf. A Physicochem. Eng. Asp. 603 (2020) 125231.

[41] M. Rbaa, M. Ouakki, M. Galai, A. Berisha, B. Lakhrissi, C. Jama, I. Warad, A. Zarrouk, Simple preparation and characterization of novel 8-Hydroxyquinoline derivatives as effective acid corrosion inhibitor for mild steel: experimental and theoretical studies, Colloids Surf. A Physicochem. Eng. Asp. 602 (2020) 125094.

[42] A.Y. Obaid, A.A. Ganash, A.H. Qusti, S.A. Elroby, A.A. Hermas, Corrosion inhibition of type 430 stainless steel in an acidic solution using a synthesized tetra-pyridinium ring-containing compound, Arab. J. Chem. 10 (2017) S1276–S1283.

[43] S.A. Mrani, S. El Arrouji, K. Karrouchi, F. El Hajjaji, K.I. Alaoui, Z. Rais, M. Taleb, Inhibitory performance of some pyrazole derivatives against corrosion of mild steel in 1.0 M HCl: electrochemical, MEB and theoretical studies, Int. J. Corros. Scale Inhib. 7 (2018) 542–569.

[44] M. Lebrini, M. Lagrenee, H. Vezin, M. Traisnel, F. Bentiss, Experimental and theoretical study for corrosion inhibition of mild steel in normal hydrochloric acid solution by some new macrocyclic polyether compounds, Corros. Sci. 49 (2007) 2254–2269.

[45] V.F. Lvovich, Impedance Spectroscopy: Applications to Electrochemical and Dielectric Phenomena, John Wiley and Sons Ltd, London, 2012, pp. 23–36.

[46] A. El yaktini, A. Lachiri, M. El Faydy, F. Benhiba, H. Zarrok, M. El Azzouzi, M. Zertoubi, M. Azzi, B. Lakhrissi, A. Zarrouk, Inhibitor effect of new azomethine derivative containing an 8-hydroxyquinoline moiety on corrosion behavior of mild carbon steel in acidic media, Int. J. Corros. Sca. Inhib. 7 (4) (2018) 609–632.

[47] L.O. Olasunkanmi, M.M. kabanda, E.E. Ebenso, Quinoxaline derivatives as corrosion inhibitors for mild steel in hydrochloric acid medium: electrochemical and quantum chemical studies, Physi. E 76 (2016) 109–126.

[48] F. Benhiba, Y. ELaoufir, M. Belayachi, H. Zarrok, A. El Assyry, A. Zarrouk, B. Hammouti, E.E. Ebenso, A. Guenbour, S.S. Al Deyab, H. Oudda, Theoretical and experimental studies on the inhibition of 1,1'-(2-phenylquinoxaline 1,4-diyl) diethanone for the corrosion of carbon steel in 1.0 M HCl, Der Pharm. Lett. 6 (4) (2014) 306–318.

[49] M.T. Majd, T. Shahrabi, B. Ramezanzadeh, Low carbon steel surface modification by an effective corrosion protective nanocomposite film based on neodymium polyacrylic acid-benzimidazole, J. Alloys. Compd. 783 (2019) 952–968.

[50] C. Verma, M.A. Quraishi, I.B. Obot, E.E. Ebenso, Effect of substituent dependent molecular structure on anti-corrosive behavior of one-pot multicomponent synthesized pyrimido [2,1-B] benzothiazoles: Computer modelling supported experimental studies, J. Mol. Liq. 287 (2019) 110972.

[51] M. Özcan, İ. Dehri, M. Erbil, Organic sulphur-containing compounds as corrosion inhibitors for mild steel in acidic media: correlation between inhibition efficiency and chemical structure, Appl. Surf. Sci. 236 (2004) 155–164.

[52] Y. Kharbach, F.Z. Qachchachi, A. Haoudi, M. Tourabi, A. Zarrouk, C. Jama, L.O. Olasunkanmi, E.E. Ebenso, F. Bentiss, Anticorrosion performance of three newly synthesized isatin derivatives on carbon steel in hydrochloric acid pickling environment: electrochemical, surface and theoretical studies, J. Mol. Liq. 246 (2017) 302–316.

[53] D.K. Yadav, D.S. Chauhan, I. Ahamad, M.A. Quraishi, Electrochemical behavior of steel/acid interface: adsorption and inhibition effect of oligomeric aniline, RSC Adv. 3 (2013) 632–646.

[54] N.A. Odewunmi, S.A. Umoren, Z.M. Gasem, Utilization of watermelon rind extract as a green corrosion inhibitor for mild steel in acidic media, J. Ind. Eng. Chem. 21 (2015) 239–247.

[55] J.J. Fu, H.S. Zang, Y. Wang, S. Li, T. Chen, X.D. Liu, Experimental and theoretical Study on the inhibition performances of quinoxaline and its derivatives for the corrosion of mild steel in hydrochloric acid, Ind. Eng. Chem. Res. 51 (18) (2012) 6377–6386.

[56] A. Zarrouk, A. Dafali, B. Hammouti, H. Zarrok, S. Boukhris, M. Zertoubi, Synthesis, characterization and comparative study of functionalized quinoxaline derivatives towards corrosion of copper in nitric acid medium, Int. J. Electrochem. Sci. 5 (2010) 46–55.

[57] A. Popova, M. Christov, Evaluation of impedance measurements on mild steel corrosion in acid media in the presence of heterocyclic compounds, Corros. Sci. 48 (2006) 3208–3221.

[58] H. Ouici, M. Tourabi, O. Benali, C. Selles, C. Jama, A. Zarrouk, F. Bentiss, Adsorption and corrosion inhibition properties of 5-amino 1,3,4-thiadiazole2-thiol on the mild steel in hydrochloric acid medium: Thermodynamic, surface and electrochemical studies, J. Electroanal. Chem. Lausanne (Lausanne) 803 (2017) 125–134.

[59] K.F. Khaled, N. Hackerman, Investigation of the inhibitive effect of *ortho*-substituted anilines on corrosion of iron in 1 M HCl solutions, Electroch. Acta 48 (2003) 2715–2723.

[60] K. Aramaki, T. Kiuchi, T. Sumiyoshi, H. Nishihara, Surface enhanced Raman scattering and impedance studies on the inhibition of copper corrosion in sulphate solutions by 5-substituted benzotriazoles, Corros. Sci. 32 (1991) 593–607.

[61] N. Anusuya, J. Saranya, P. Sounthari, A. Zarrouk, S. Chitra, Corrosion inhibition and adsorption behaviour of some bis-pyrimidine derivatives on mild steel in acidic medium, J. Mol. Liq. 225 (2017) 406–417.

[62] A. Tazouti, M. Galai, R. Touir, M. Ebn Touhami, A. Zarrouk, Y. Ramli, M. Saraçoğlu, S. Kaya, F. Kandemirli, C. Kaya, Experimental and theoretical studies for mild steel corrosion inhibition in 1.0 M HCl by three new quinoxalinone derivatives, J. Mol. Liq. 221 (2016) 815–832.

[63] M. Prabakaran, S.-H. Kim, K. Kalaiselvi, V. Hemapriya, I.-M. Chung, Highly efficient *Ligularia fischeri*green extract for the protection against corrosion of mild steel in acidic medium: Electrochemical and spectroscopic investigations, J. Taiwan Inst. Chem. Eng. 59 (2016) 553–562.

[64] M.R. Gholamhosseinzadeh, H. Aghaie, M. Shahidi Zandib, M. Giahi, Rosuvastatin drug as a green and effective inhibitor for corrosion of mild steel in HCl and H_2SO_4 solutions, J. Mater. Res. Technol. 8 (6) (2019) 5314–5324.

[65] M. Mobin, M. Rizvi, Adsorption and corrosion inhibition behavior of hydroxyethyl cellulose and synergistic surfactants additives for carbon steel in 1 M HCl, Carbohydr. Polym. 156 (2017) 202–214.

[66] P. Mourya, P. Singh, A.K. Tewari, R.B. Rastogi, M.M. Singh, Relationship between structure and inhibition behaviour of quinolinium salts for mild steel corrosion: experimental and theoretical approach, Corros. Sci. 95 (2015) 71–87.

[67] A. Salhi, S. Tighadouini, M. El-Massaoudi, M. Elbelghiti, A. Bouyanzer, S. Radi, S. El Barkany, F. Bentiss, A. Zarrouk, Keto-enol heterocycles as new compounds of corrosion inhibitors for carbon steel in 1 M HCl: weight loss, electrochemical and quantum chemical investigation, J. Mol. Liq. 248 (2017) 340–349.

[68] P. Mourya, S. Banerjee, M.M. Singh, Corrosion inhibition of mild steel in acidic solution by Tagetes erecta (Marigold flower) extract as a green inhibitor, Corros. Sci. 85 (2014) 352–363.

[69] N.O. Eddy, Experimental and theoretical studies on some amino acids and their potential activity as inhibitors for the corrosion of mild steel, part 2, J. Adv. Res. 2 (1) (2011) 35–47.
[70] O. Dagdag, A. Berisha, Z. Safi, S. Dagdag, M. Berrani, S. Jodeh, C. Verma, E.E. Ebenso, A. El Harfi, Highly durable macromolecular epoxy resin as anticorrosive coating material for carbon steel in 3% NaCl: computational supported experimental studies, J. Appl. Polym. Sci. (2020) 49003 doi.org/10.1002/app.49003.
[71] L.M. Rodríguez-Valdez, W. Villamisar, M. Casales, J.G. Gonzalez-Rodriguez, A. Martínez-Villafañe, L. Martinez, D. Glossman-Mitnik, Computational simulations of the molecular structure and corrosion properties of amidoethyl, aminoethyl and hydroxyethyl imidazolines inhibitors, Corros. Sci. 48 (12) (2006) 4053–4064.
[72] A. Berisha, F. Podvorica, V. Mehmeti, F. Syla, D. Vataj, Theoretical and experimental studies of the corrosion behavior of some thiazole derivatives toward mild steel in sulfuric acid media, Maced. J. Chem. Chem. Eng. 34 (2) (2015) 287–294.
[73] R. Hsissou, B. Benzidia, M. Rehioui, M. Berradi, A. Berisha, M. Assouag, N. Hajjaji, A. Elharfi, Anticorrosive property of hexafunctional epoxy polymer HGTMDAE for E24 carbon steel corrosion in 1.0 M HCl: gravimetric, electrochemical, surface morphology and molecular dynamic simulations, Polym. Bull. Berl. (Berl) (2019) doi.org/10.1007/s00289-019-02934-02935.
[74] H.M. Abd El-Lateef, K.A. Soliman, A.H. Tantawy, Novel synthesized Schiff Base-based cationic gemini surfactants: electrochemical investigation, theoretical modeling and applicability as biodegradable inhibitors for mild steel against acidic corrosion, J. Mol. Liq. 232 (2017) 478–498.
[75] M.M. Khalaf, A.H. Tantawy, K.A. Soliman, H.M. Abd El-Lateef, Cationic gemini-surfactants based on waste cooking oil as new 'green' inhibitors for N80-steel corrosion in sulphuric acid: a combined empirical and theoretical approaches, J. Mol. Struct. 1203 (2020), https://doi.org/10.1016/j.molstruc.2019.127442.